frontiers | Frontiers in Environmental Science

TYPE Original Research
PUBLISHED 11 October 2022
DOI 10.3389/fenvs.2022.1024797

OPEN ACCESS

EDITED BY
Chengcheng Li,
China University of Geosciences
Wuhan, China

REVIEWED BY
Zhuanxi Luo,
Huaqiao University, China
Zheng Zhang,
China University of Mining and
Technology, China
Yimin Sang,
Beijing Institute of Petrochemical
Technology, China

*CORRESPONDENCE
Herong Gui,
guiherong@163.com

SPECIALTY SECTION
This article was submitted to Freshwater
Science,
a section of the journal
Frontiers in Environmental Science

RECEIVED 22 August 2022
ACCEPTED 26 September 2022
PUBLISHED 11 October 2022

CITATION
Hao C, Wang Y, He K and Gui H (2022),
Seasonal distribution of deep
groundwater fluoride, geochemical
factors and ecological risk for irrigation
in the Shendong mining area, China.
Front. Environ. Sci. 10:1024797.
doi: 10.3389/fenvs.2022.1024797

Seasonal distribution of deep groundwater fluoride, geochemical factors and ecological risk for irrigation in the Shendong mining area, China

Chunming Hao[1,2,3], Yantang Wang[3], Kaikai He[3] and Herong Gui[2]*

[1]State Key Laboratory of Coal Resources and Safe Mining, Beijing, China, [2]Key Laboratory of Mine Water Resource Utilization of Anhui Higher Education Institutes, Suzhou University, Suzhou, China, [3]North China Institute of Science and Technology, Sanhe, China

High-fluoride (F^-) deep groundwater in the vicinity of mining areas poses severe ecological risks. In this study, we aimed to characterize and reveal the seasonal distribution and influencing factors of elevated F^- concentrations in the deep groundwater in the Shendong mining area, Shaanxi and Inner Mongolia province, China. In addition, the ecological risks associated with F^- concentrations in irrigation water were assessed. During the wet and dry seasons, the F^- concentrations in mine water samples ranged between 0.12 and 13.92 mg/L (mean: 4.24 mg/L) and between 0.20 and 17.58 mg/L (mean: 4.59 mg/L), respectively. The F^- content of mine water was clearly higher during the dry season than that during the wet season. F^- concentrations in deep groundwater exhibited consistent spatial distributions during both the dry and wet seasons, with an evident increase from southeast to northwest. The dissolution and precipitation of F^--bearing and calcium minerals, cation exchange, competitive adsorption, evaporation, and anthropogenic activities during both the wet and dry seasons were identified as important factors influencing F^- concentrations in deep groundwater. In addition, the ecological assessment revealed that 100% and 88.89% of low-F^- deep groundwater samples were suitable for practices during the dry and wet seasons, respectively. In contrast 84.00% and 84.62% of high-F^- deep groundwater samples were unsuitable for irrigation practices during the dry and wet seasons, respectively. This research provided useful prevention policies of deep groundwater extraction to mitigate environment problems associated with excessive F^- irrigation.

KEYWORDS

fluoride, seasonal distribution, geochemical factors, ecological assessment, deep groundwater

Introduction

Fluorine (F), one of the lightest halogen elements in the environment, is difficult to precipitate under normal temperature and pressure conditions and typically occurs as fluoride (F^-) in natural water (Ali et al., 2018). For emerging countries such as China and India, potable groundwater is the primary source of F^- consumption (Aghapour et al., 2018; Ali et al., 2018; Adeyeye et al., 2021; Araya et al., 2022). It is well known that the concentration of F^- has an effect on human health. F^- concentrations in natural water sources are typically less than 1.00 mg/L (Laxmankumar et al., 2019; LaFayette et al., 2020). Long-term consumption of potable groundwater containing F^- concentrations greater than 1.00 mg/L and 4.00 mg/L can cause dental and skeletal fluorosis, respectively (Kumar et al., 2018; LaFayette et al., 2020). In addition, a high concentration (>10.00 mg/L) of F^- is commonly associated with carcinogenic effects, including arthritis, neurological disorders, thyroid cancer, infertility, and hypertension (Ali et al., 2018; Toolabi et al., 2021; Chicas et al., 2022; Hao et al., 2022). Hence, it is safe to consume potable groundwater with F^- concentration below 1.00 mg/L, which is the maximum permissible F^- concentration for drinking water in China (He J et al., 2013; Hao et al., 2021a). Prior to consumption, the pre-treatment processes that regulate the F^- concentration in groundwater are considered essential. Groundwater is also the primary source of irrigation water in arid and semi-arid regions around the world, ensuring specific crop yields (Kumar et al., 2018; Kumar et al., 2019; Li et al., 2021).

The two principal sources of F^- in groundwater are anthropogenic (Borzi et al., 2015; Mamatchi et al., 2019; Su et al., 2021; Yadav et al., 2021; Zango et al., 2021; Huang et al., 2022) and geogenic in origin (Currell et al., 2011; He X et al., 2013; Xiao et al., 2015; Dehbandi et al., 2018; Hao et al., 2021b; Duggal and Sharma, 2022). Previous studies have found that geogenic processes are frequently responsible for elevated F^- concentrations in groundwater (Dehbandi et al., 2018; Emenike et al., 2018; Rashid et al., 2018; Hao et al., 2021c; Duggal and Sharma, 2022; Huang et al., 2022). Importantly, F-bearing minerals in rock strata, including fluorite, fluorapatite, and cryolite, are typically identified as the most important geogenic sources of F^- (He J et al., 2013; Mondal et al., 2014; Olaka et al., 2016; Laxmankumar et al., 2019; Hao et al., 2021d; Duggal and Sharma, 2022; Rehman et al., 2022). In addition, specific water-rock interactions play a very important role in the fluoride enrichment of groundwater, such as evaporation (Dehbandi et al., 2018; Li et al., 2018; Chicas et al., 2022; Rehman et al., 2022), competitive adsorption (Li et al., 2018; Ali et al., 2019; Rehman et al., 2022), and ion exchange effects (Li et al., 2015; Ali et al., 2018; Huang et al., 2022; Nizam et al., 2022). Anthropogenic sources, such as application of phosphate fertilisers and pesticides, use of aluminum smelting, glass and brick industries, the burning of coal, and processing of mining activities, also contribute excessive amounts of fluoride into groundwater (Li et al., 2018; Rashid et al., 2018; Ali et al., 2019; Hao et al., 2022; Zhang et al., 2022). Furthermore, numerous geochemical ions may affect the presence of F^- in groundwater. For instance, high-F^- groundwater often have neutral to alkaline pH and they are typically Na-HCO_3 dominant with low concentrations of Ca^{2+} and Mg^{2+} (Li et al., 2018; LaFayette et al., 2020; Huang et al., 2022; Nizam et al., 2022).

The exploitation of underground coal resources is always accompanied by the drainage of vast quantities of mine water (Yang et al., 2019; Yuan et al., 2022). Excessive mining activities and their associated mine water drainage are unavoidable sources of several geogenic elements such as F^- and other pollutants (Jeong et al., 2018; Blasco et al., 2019; Yadav et al., 2021). F^- has been previously detected in coal and categorized as a toxic element (He J et al., 2013; Yadav et al., 2021; Hao et al., 2022) and coal mines activities usually incorporate toxic elements into mine water (Yadav et al., 2021). The discharge of untreated F^--containing mine water from coal mines typically contaminates the surrounding groundwater system and leads to environmental degradation (Yadav et al., 2021; Zhang et al., 2021; Zhang et al., 2022). Due to various geochemical factors, the seasons influence the F^- concentrations in groundwater differently (Orland et al., 2014; Najamuddin et al., 2016; Sahu et al., 2020). Owing to the negative effects of high-F^- mine water, it is of the utmost importance to monitor the seasonal quality of groundwater in arid and water-scarce areas from an ecological perspective. As one of the eight largest coalfields in the world, the Shendong mining area annually discharges approximately 106 million tons of mine (Hao et al., 2021a; Xu et al., 2021; Zhang et al., 2021). Several studies have indicated that the F^- concentration in mine water of part of the Shendong mining area exceeds 1.00 mg/L, which unquestionably poses environmental risks (Hao et al., 2021b; Guo et al., 2021; Zhang et al., 2021; Hao et al., 2022). The large amount of groundwater with high fluoride is not suitable for domestic water, due to lack appropriate treatment technology and adequate funding (Gu, 2014; Gu et al., 2021). Hence, the high-F^- groundwater primarily guarantees the water supply for ecological irrigation for the natural fragilely ecological conditions (Gu, 2014; Gu et al., 2021) and for landscape water after simple purification treatment (Song et al., 2020), which doubtlessly brings potential crises for the ecological environment of the mining area. Although the spatial distribution, geochemical behavior, and formation mechanisms for elevated F^- in mine water in the Shendong mining areas have been investigated (Hao et al., 2021c; Zhang et al., 2021; Hao et al., 2022), the impact of high-F^- mine water, seasonal effects, and ecological irrigation risks of F^- concentrations on the surrounding deep groundwater have received limited attention. Moreover, assessing the F^- concentrations in deep groundwater during the dry and wet seasons is beneficial for analyzing the seasonal concentration changes and determining the ecological irrigation risks.

In this study, we aimed to 1) further investigate the spatial characteristics and influencing factors of deep groundwater F^- in the vicinity of the Shendong mining area during the dry and wet seasons; and 2) assess the ecological irrigation risks associated with F^- concentrations in deep groundwater using the sodium adsorption ratio (SAR) and sodium percentage (Na%). The results of this study contributed to a comprehensive understanding of the seasonal distribution and geochemical factors of F^- in deep groundwater affected by mining activities, thereby preventing ecological impacts associated with excessive F^- irrigation in the Shendong mine area.

Geological background

The Shendong mining area (geographical coordinates: 111°04′–111°11′ N and 39°20′–39°30′ E) is located in a mountainous region and spans a surface area of 3481 km^2 (Figure 1). This region has a typical warm-temperate and semi-arid continental monsoon climate and recorded an average annual precipitation rate of approximately 437.2 mm and an average annual evaporation rate of 2065.1 mm between 1949 and 2012. The average temperature is 9.9°C. As a component of the Ulan Mulun River system, no major rivers transect the mining area.

The overall geological structure of the Shendong mining area is a monocline dipping towards the SW with a dip angle of 1–8°. Faults are rare in the mining areas and the geologic structure is identified as simple (Zhang et al., 2021; Hao et al., 2022). Usually, Yanchang Formation (T_{3y}) of the Upper Triassic, Fuxian Formation (J_{1f}) of the Lower Jurassic, Yanan Formation ($J_{1\text{-}2y}$) of the Middle and Lower Jurassic, Zhiluo Formation (J_{2z}) and Anding Formation (J_{2a}) of the Middle Jurassic, Cenozoic (K_z) and Salawusu Formation (Q_{3s}) are the main geological strata from bottom to top in the Shendong mining area (Zhang et al., 2021). The Q_{3s} phreatic (shallow groundwater) and $J_{1\text{-}2y}$ deep groundwater (deep groundwater) aquifers are the main aquifers in the mining area. Owing to their thickness (119.09–227.12 m, mean: 174.93 m) and relative abundance of water, deep groundwater aquifers are an essential source of potable and irrigation water in the area. The lithology of the deep groundwater aquifers is predominantly medium-coarse sandstones with a small amount of siltstone. There are extensive amounts of F^- and silicate minerals in the rock stratum and the fractures are poorly developed. The deep groundwater has hydraulic conductivity from 0.002 to 0.016 m/d, and belongs to a weak water-rich aquifer. Unpolluted water aquifers principally have hydrochemical facies of Na-HCO_3 and Na-HCO_3-Cl. Deep groundwater is primarily recharged through precipitation infiltration and partially recharged through shallow groundwater leakages.

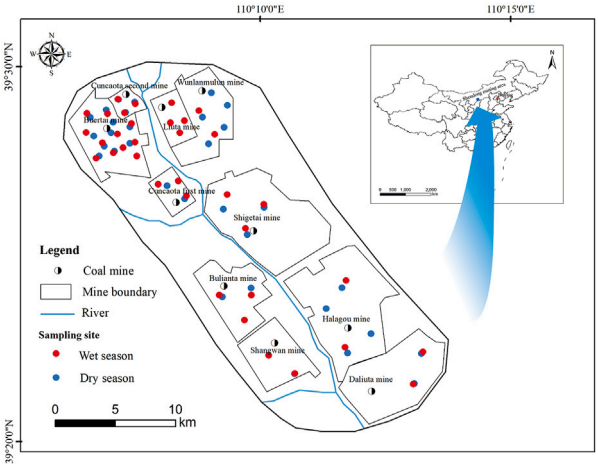

FIGURE 1
Location of Shendong mining area in China and distribution of deep groundwater sampling sites.

Groundwater flows from south to north *via* sandstone fissures and mainly drains out through springs and burnt rocks aquifer.

The deep groundwater aquifer contains abundant coal reserves, and the recoverable coal seams consist of No. 1^{-2}, 2^{-2}, 3^{-1}, 4^{-2}, and 5^{-2} coal seams with an average thickness of 4–6 m (Xu et al., 2021; Zhang et al., 2021; Hao et al., 2022). The surface of the mining area is covered by scattered surface materials, sparse vegetation, a dry environment, and windblown sand, with a thickness of 20–50 m (Zhang et al., 2021). In the mining area, water erosion and wind erosion are widespread and intense, and soil and water loss are severe issues (Xiao et al., 2020). Agriculture is uncommon in the Shendong mine area, where psammophytes and xerophytes are the dominant ecological plants.

Materials and methods

Sample collection

A total of 35 deep groundwater samples were collected from drilling holes and monitoring wells in the dry (December 2020) and wet (August 2020) seasons (Figure 1). Before collection, brown ampoules were washed 2–3 times, first with distilled and then with sample water. The sample water was then filtered *via* 0.45 μm glass fiber membranes prior to collection. Two 500 ml samples were collected from each sampling location for cation and anion analyses. Meanwhile, 5.00 ml of F^- recovery indicator (1.00 mg/L) was added to and mixed with the cation

TABLE 1 The classification statistics of SAR and Na% irrigation suitability.

Parameter	Range	Grade
Sodium adsorption ratio (SAR)	<10	Low (suitable)
	10–18	Medium (more suitable)
	19–26	High (not suitable)
	>26	Very high (not suitable)
Sodium percentage (Na%)	<20	Low (suitable)
	20–40	Medium (more suitable)
	40–60	High (not suitable)
	>60	Very high (not suitable)

analysis sample. Total dissolved solids (TDS) and pH values were measured *in situ*.

Sample analysis

Calcium, magnesium, sodium, and potassium concentrations were measured using inductively coupled plasma-atomic emission spectrometry (ICP-OES; Agilent 7900, United States). The concentrations of F^-, chloride, and sulfate were determined by ion chromatography (Dionex Integrion IC, Thermo Fisher, United States). Nitrates and ammonia-nitrogen were determined by spectrophotometry (Multiskan SkyHigh, United States). The concentrations of bicarbonate and carbonate were determined using acid-base titration. The pH and TDS values were obtained using a portable pH meter (HANNA H18424, Italy) and a portable electrical conductivity meter (HANNA H1833, Italy), respectively.

Each reported value was the average of three test results, with a relative standard deviation below 10%. The detection limit of bicarbonate and carbonate analyses was 0.1 mg/L, whereas all other ion analyses had a detection limit of 0.01 mg/L. Recovery rates of 95%–105% for F^- concentration were determined. The absolute ionic balance errors of the analyzed water samples were generally around 5%. Moreover, approximately 20% of the water samples were randomly re-analyzed to ensure that the relative deviation qualification rate exceeded 90%.

Assessment of irrigation water quality

The quality of deep groundwater for irrigation was evaluated using the SAR and Na% methods.

The SAR and Na% were estimated using Eqs 1, 2:

$$\mathbf{SAR} = \mathbf{Na^+} \Big/ \sqrt{\mathbf{Ca^{2+}} + \mathbf{Mg^{2+}}} \quad (1)$$

$$\mathbf{Na\%} = (\mathbf{Na^+} + \mathbf{K^+}) \Big/ (\mathbf{Ca^{2+}} + \mathbf{Mg^{2+}} + \mathbf{Na^+} + \mathbf{K^+}) \times \mathbf{100} \quad (2)$$

where each ion was measured in meq/L. Table 1 displays the classification statistics for the SAR and Na% irrigation suitability of deep groundwater.

Statistical analysis

Origin 2021 software was used for data description and statistical analysis. Piper and Gibbs diagrams were used to elucidate the hydrogeochemical facies and processes. The spatial variance of F^- in groundwater was evaluated using the inverse distance weight method within ArcGIS 9.3. The geochemical model PHREEQC was used to calculate the

TABLE 2 Geochemistry data in deep groundwater for wet and dry season.

Types	mg/L											pH
	F^-	Cl^-	HCO_3^-	SO_4^{2-}	NO_3^-	K^+	Ca^{2+}	Mg^{2+}	Na^+	NH_4^+	TDS	
Wet season (n = 35)												
Min	0.12	5.52	135.2	3.05	0.00	0.10	1.03	0.46	8.90	0.00	198	7.02
Max	13.92	969.00	1460.0	1035.60	8.10	11.50	104.15	52.70	1754.20	2.11	3842	9.70
Mean	4.40	171.33	492.4	171.53	1.25	3.95	29.63	6.54	335.01	0.20	1021	8.12
SD	3.72	186.41	348.1	252.67	1.48	2.83	26.68	10.07	310.83	0.38	666	0.58
Dry season (n = 35)												
Min	0.20	6.07	155.2	6.04	0.00	0.12	0.58	0.61	5.01	0.00	182	7.05
Max	17.58	425.70	1526.5	910.10	8.17	13.00	72.82	29.86	998.30	2.57	2874	8.50
Mean	4.94	157.00	617.2	184.54	1.42	4.57	22.54	8.05	385.68	0.26	1351	7.86
SD	4.18	137.28	337.6	178.56	1.77	3.30	23.79	7.71	243.10	0.56	721	0.45

Values less than LOD (limit of detection) were set to zero for statistical purposes.

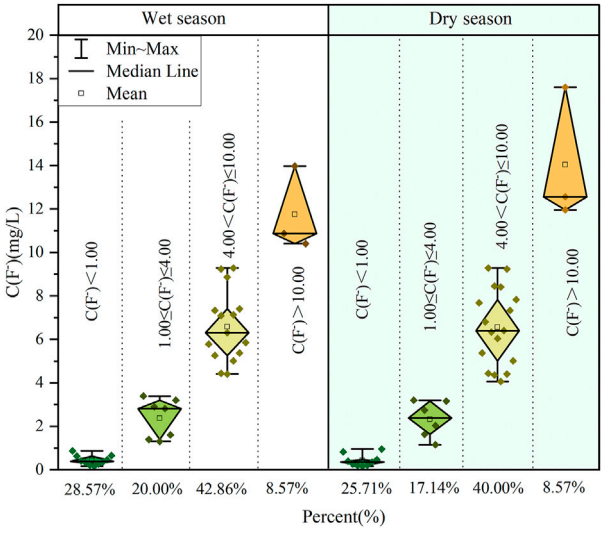

FIGURE 2
The percent boxplots of F^- content during the wet and dry seasons.

saturation index (SI) values to assess the degree of equilibrium between the water and minerals. The geochemical data for deep groundwater are contained in Table 2.

Results

Fluoride concentration of deep groundwater

The F^- concentrations in deep groundwater ranged between 0.12 and 13.92 mg/L (mean: 4.40 ± 3.72 mg/L) in the wet season (Table 2). Approximately 65.71% of deep groundwater samples exhibited F^- concentrations that exceeded the drinking water guidelines in China (i.e., 1.00 mg/L). Deep groundwater had higher F^- concentrations during the dry season than those during the wet season, ranging from 0.20 to 17.58 mg/L (mean: 4.94 ± 4.18 mg/L). Notably, 74.29% of the deep groundwater samples had F^- concentrations exceeding 1.00 mg/L. The mean F^- concentration of deep groundwater during the dry season was 1.12 times that during the wet season, suggesting that inhabitants who consume this water face a greater risk of developing fluorosis during the dry season.

Considering the drinking water guidelines in China and the health risk of fluorosis (Toolabiet al., 2021; Hao et al., 2022), the deep groundwater samples were divided into four groups: below 1.00 mg/L (low-F^- deep groundwater), 1.00–4.00 mg/L, 4.00–10.00 mg/L, and above 10.00 mg/L. All the F^- concentrations recorded in deep groundwater that exceeded 1.00 mg/L were designated as high-F^- deep groundwater. The

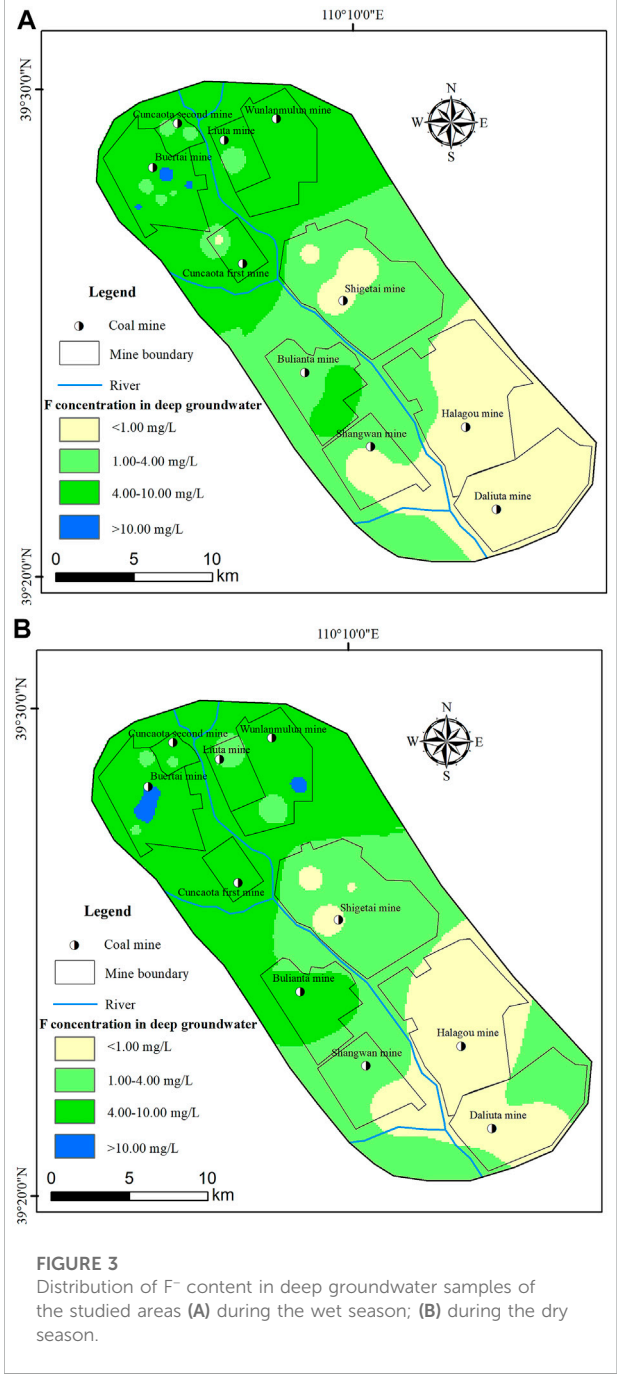

FIGURE 3
Distribution of F^- content in deep groundwater samples of the studied areas **(A)** during the wet season; **(B)** during the dry season.

range of F^- concentrations for deep groundwater samples with below 1.00 mg/L, 1.00–4.00 mg/L and 4.00–10.00 mg/L were identical in both wet and dry seasons (Figure 2). Compared with wet season, the F^- concentration was markedly increased in the deep groundwater with F^- concentrations above 10.00 mg/L and the mean F^- concentration was 1.21 times during the dry season, indicating that seasonal variation played a significant role in the enrichment of F^- in deep groundwater samples with F^- concentrations above 10.00 mg/L.

The mapping of F^- concentrations in deep groundwater revealed consistent spatial variations between the dry and wet seasons, with the fluoride concentrations of mine waters clearly increasing from the southeast to northwest (Figure 3). In particular, the Buertai mine area had the highest F^- concentrations in deep groundwater, measuring 13.92 mg/L during the wet season and 17.58 mg/L during the dry season. The results were identical to the studies of the spatial distribution of mine water reported by Hao (2022) and Zhang (2021), indicating that the F^- concentrations of deep groundwater may be significantly impacted by coal mining activities.

Geochemical characterization

As shown in Table 2, pH values of the deep groundwater in the Shendong mining area ranged from 7.02 (i.e., neutral) to 9.70 (i.e., alkaline), with a mean of 8.12 ± 0.58 in the wet season. Moreover, the pH values ranged from 7.05 to 8.50, with an average of 7.86 ± 0.45, in the dry season. TDS values of deep groundwater exceeded the acceptable limit for drinking water of 1000 mg/L by approximately 40.00% and 54.29% in the wet and dry seasons, respectively. The mean TDS concentration of deep groundwater during the dry season was higher than that during the wet season, indicating that the water-rock interaction process in deep groundwater was relatively stronger (Guo and Wang, 2005; Jakóbczyk-Karpierz et al., 2017; Hao et al., 2021a).

Deep groundwater samples in the study area were mainly located in the bottom right of the piper diagram, with the predominant hydrochemical types being the Na-HCO_3-Cl (52.00%) and Na-HCO_3-SO_4 (28.00%) types in the wet season, and Na-HCO_3-Cl (53.85%) and Na-HCO_3-SO_4 (30.77%) types in the dry season (Supplementary Figure S1). In addition, the high-F^- deep groundwaters were either the Na-HCO_3-Cl or Na-HCO_3-SO_4 types, with Na-types constituting the overwhelming majority. The low- F^- deep groundwaters had various proportions of Ca-HCO_3, Ca-SO_4-Cl, Na-HCO_3, and Na-HCO_3-Cl types, with 56% Ca-type and 44% Na-type. The results demonstrated that the transition from Ca-types to Na-types was advantageous for the enrichment of F^- concentrations in deep groundwater (Liu et al., 2021; Zhang et al., 2021).

Geochemical factors controlling fluoride in deep groundwater

Generally, understanding the relationship between F^- and geochemical elements in deep groundwater is essential to gain deeper insight into fluoride behavior (Li et al., 2015; Laxmankumar et al., 2019; Liu et al., 2021; Toolabi et al., 2021).

In Figure 4, deep groundwater F^- had a strongly negative correlation with Mg^{2+} (R^2 = −0.66) and Ca^{2+} (R^2 = −0.84), and a significantly positive correlation with pH (R^2 = 0.82), Cl^- (R^2 = 0.85),

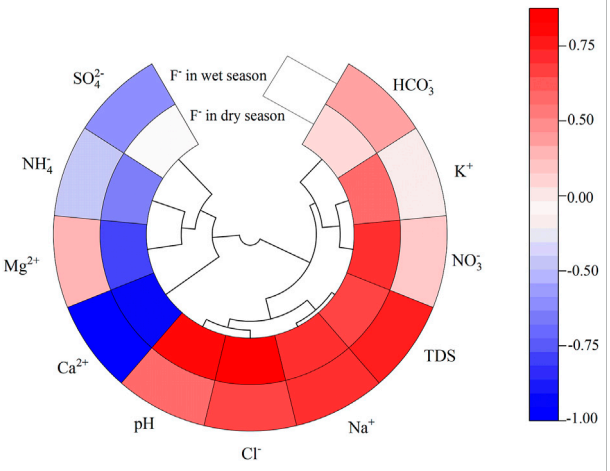

FIGURE 4
Relationships between F^- content and the geochemical elements in deep groundwater during the wet and dry seasons.

Na^+ (R^2 = 0.72), TDS (R^2 = 0.69), and NO_3^- (R^2 = 0.74), in the dry season. However, high TDS (R^2 = 0.86), Na^+ (R^2 = 0.77), Cl^- (R^2 = 0.68) and low Ca^{2+} (R^2 = −0.87) concentrations were the primary limiting geochemical factors for F^- during the wet season. Notably, the similar effect relationship between F^- and Ca^{2+}, Na^+, TDS, and Cl^- during both the dry and wet seasons indicated that Ca^{2+}, Na^+, TDS, and Cl^- had a significant effect on F^- concentrations in deep groundwater in the study area. However, the effect of pH, Mg^{2+}, and NO_3^- on F^- concentrations may have explained why F^- content increased more during the dry season than during the wet season.

Discussion

As shown in Figure 5A, there was a significantly negative correlation between F^- and Ca^{2+} during the wet and dry seasons in the Shendong mining area, indicating that the dissolution of F-bearing minerals was one of the major factors influencing the enrichment of F^- in deep groundwater (Hao et al., 2021b; Chen et al., 2021; Noor et al., 2022). All deep groundwater samples collected during the wet and dry seasons were distributed towards the saturated dissolution line of fluorite (K_{SP} = $10^{-10.6}$), further demonstrating that the dissolution of fluorite had a substantial effect on the appearance of high-F^- deep groundwater. Therefore, as the Ca^{2+} content rapidly increased, the F^- content would accelerate the reduction. The dissolution process of fluorite minerals was as follows:

$$\mathbf{CaF_2 \rightarrow Ca^{2+} + 2F^-} \quad (3)$$

The geology of the study area, as defined by Zhao and Wei, 2020; Duan et al., 2021, includes extensive F-bearing minerals

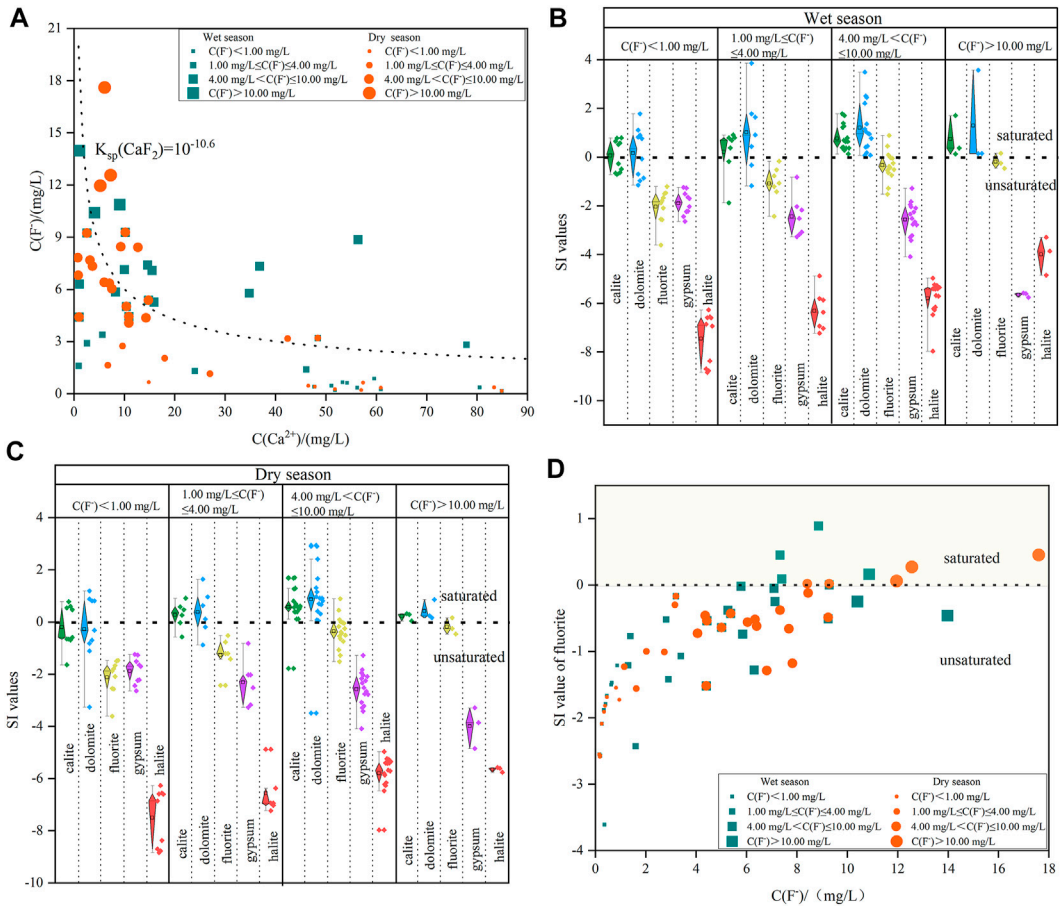

FIGURE 5
The plots of: **(A)** Ca^{2+} *versus* the F^- content; **(B)** the boxplots of SI values of minerals during the wet season; **(C)** the boxplots of SI value of minerals during the dry season; **(D)** the $SI_{fluorite}$ *versus* the F^- content in deep groundwater.

such as fluorite (CaF_2), muscovite ($KAl_3(AlSi_3O_{10})F_2$) and biotite ($KMg_3(AlSi_3O_{10})F_2$) in the J_{1-2y} stratum. Long-term water-rock interaction with F-bearing minerals inevitably increased enrichment of F^- in deep groundwater. Although the F^- concentration in deep groundwater was largely dependent on the rate and degree of fluorite dissolution, a precipitate state of calcium minerals such as calcite and dolomite could decrease Ca^{2+} concentrations and accelerate the promotion of F^- concentrations (Li et al., 2018; Noor et al., 2022). The SI values of calcium minerals could provide a thorough explanation of this process. The proportions of low-F^- deep groundwater samples showing negative SI values for calcite and dolomite were 55.56% and 55.56%, respectively, during both wet and dry seasons. However, the proportions of high-F^- deep groundwater samples showing negative SI values were 11.54% and 15.38%, respectively, during both dry and wet seasons (Figure 5B). Moreover, all deep groundwater samples with F^- concentrations above 10.00 mg/L were oversaturated with dolomite and calcite, demonstrating that the precipitation of dolomite and calcite can promote the dissolution of fluorite, resulting in an elevated F^- content in deep groundwater owing to a low Ca^{2+} content (Rafique et al., 2015; Rashid et al., 2018; Thapa et al., 2018).

Similarly, as depicted in Figures 5B,C, the SI values of fluorite during the dry season ranged between -2.59 and 1.54, with a mean of -0.83, whereas the SI values of fluorite during the wet season ranged between -3.61 and 0.89, with a mean of -0.65. The proportions of all deep groundwater samples showing positive $SI_{fluorite}$ values were 17.14% and 14.29% during the wet and dry seasons, respectively. This indicated that the majority of fluorite in the study area was in an unsaturated state and tended to continue dissolving. The positive correlation identified between F^- and $SI_{fluorite}$ (Figure 5D) were observed in both the wet and dry seasons for deep groundwater, further indicating that fluorite dissolution was the key driving agent for the elevation of F^- concentrations (Eang et al., 2018; Wu et al., 2018).

Higher HCO_3^- concentrations and alkaline pH values promoted the release of F^- into groundwater (Ali et al., 2018;

Ali et al., 2019; Wang et al., 2021). It is well known that the concentration of HCO_3^- increases as the pH increases, hence the F^-concentration in a constant pH (7.00–8.33) groundwater environment is often dominated by HCO_3^-. As shown in Table 2, 74.28% and 82.86% of deep groundwater samples had pH ranges of 7.00–8.33 during the wet and dry seasons, respectively. In this study, deep groundwater samples overall have a relatively lower average pH value during the dry season than that during the wet season, indicating higher F^- concentration may have other sources in deep groundwater during the dry season. Correspondingly, the mean SO_4^{2-} concentration (184.54 ± 178.56 mg/L) of deep groundwater during the wet season is less than that during the dry season in Table 2. A previous study (Hao et al., 2022) had showed that the oxidation of pyrite in a coal seam can generate SO_4^{2-} concentration enrichment, and then prevent the precipitation of CaF_2, promoting higher F^- content in deep groundwater.

Previous studies had revealed that pH values of 7.40–9.60 can make the surface charge of the clay minerals (e.g., muscovite and biotite) neutral or slightly negative and inhibit the adsorption of negatively charged F^- ions (Singh et al., 2011; Guo et al., 2012; Xiao et al., 2015). In addition, F^- and OH^- frequently replace each other on the mineral surfaces with similar ionic radii when the aqueous environment is favorable (Currell et al., 2011; Xiao et al., 2015). Compared to the wet season, the correlation between fluoride concentration and pH was positively stronger during the dry season (Figure 4), indicating pH played a significant role in F^- concentration elevations during the dry season. Therefore, the OH^- replaced the exchangeable F^- on the surfaces of clay minerals throughout the dry season, increasing the F^- concentrations in deep groundwater.

The process could be described by Eqs 4, 5:

$$KAl_3(AlSi_3O_{10})F_2 + 2OH^- \rightarrow KAl_2(AlSi_3O_{10})(OH)_2 + 2F^- \quad (4)$$

$$KMg_3(AlSi_3O_{10})F_2 + 2OH^- \rightarrow KMg_3(AlSi_3O_{10})(OH)_2 + 2F^- \quad (5)$$

During the dry season, the observed relationship between F^- and HCO_3^- has a poor correlation ($R^2 = 0.16$) in Figure 4, whereas competitive absorption was a contributing factor in F^- desorption in deep groundwater cannot be ignored. Ali et al. (2019) and Guo et al. (2012) confirmed that the presence of HCO_3^- would reduce the number of available absorbent sites and lead to the release of F^- from clay minerals, consequently increasing the F^- concentration in deep groundwater.

The poor correlation between F^- and HCO_3^- during the dry season.

There was a moderately positive correlation ($R^2 = 0.74$) between F^- and NO_3^- during the dry season (Figure 4). Previous studies showed that groundwater with high F^- concentrations typically had low NO_3^- concentrations (>5 mg/L) (Hao et al., 2021c; Li et al., 2021; Mwiathi et al., 2022). The presence of more than 5 mg/L NO_3^- in 36% of the high-F- deep groundwater indicated the impacts of anthropogenic activities such as fertilizer application and waste discharge from agricultural, domestic, and industrial sources (Ali et al., 2019; Su et al., 2021; Yadav et al., 2021). The highest observed deep groundwater NO_3^- concentration was 8.17 mg/L in the Buertai mining area. The entry of polluted mine water into the deep groundwater aquifer system promoted the enrichment of F^- concentrations *via* goaf fissures (Song et al., 2020; Zhang et al., 2021). The weak correlation ($R^2 = 0.19$) between F^- and NO_3^- during the wet season further suggested that anthropogenic activities were not the main contributor to high F^- levels in deep groundwater.

F^- positively correlated with Na^+ during both dry and wet season in deep groundwater (Figure 4). Cation exchange between Ca^{2+} and Na^+ was regarded as one of the primary sources of groundwater Na^+; therefore, the relationship between Cl^- - Na^+ - K^+ and HCO_3^- + SO_4^{2-} - Ca^{2+} - Mg^{2+} was extensively used to determine the cation exchange process in deep groundwater (Li et al., 2015; Ali et al., 2019; Liu et al., 2021). As shown in Figure 6, most deep groundwater samples were distributed along the 1:1 line during both the dry and wet seasons, indicating that the cation exchange process had an important influence on the F^- contents (Liu et al., 2021; Hao et al., 2022). Deep groundwater samples from both the wet and dry seasons were close to the 1:1 line and had high correlations with R^2 of 0.80 and 0.84, respectively. This suggested that the ion exchange reaction was more intense during the wet season than during the dry season. The results may explain why the concentration of F^- in deep groundwater was greater during the dry season than that during the wet season. The increase in Na^+ and decrease in Ca^{2+} concentrations in deep groundwater are typically caused by cation exchange reactions. Clay minerals (e.g., illite and kaolinite) are plentiful in the J_{1-2y} stratum, which contains abundant exchange sites for the displacement of Na^+ by Ca^{2+}. For convenience, the reaction process was represented by Eq. 6:

$$2NaX + Ca^{2+} \rightarrow 2Na^+ + CaX_2 \quad (6)$$

Therefore, as Ca-type water changed to Na-type water in the system, the Ca^{2+} concentration reduction accelerated the dissolution of fluorite and consequently released additional F^- into deep groundwater.

Two chloroalkaline ion exchange indices (CAI) are also evaluated whether ion exchanges occurring between Na^+ in the groundwater and Ca^{2+} in the stratum using the Eqs 7, 8. If both values of CAI 1 and CAI 2 are all positive, the Na^+ in groundwater have been exchanged for Ca^{2+} in the stratum. In contrast, if both values of CAI 1 and CAI 2 are negative, the Ca^{2+} in groundwater have been exchanged by Na^+ in the stratum. Moreover, the larger the absolute values of CAI, the stronger the ion exchange interaction (Li et al., 2015; Dehbandi et al., 2018; Hao et al., 2022).

$$CAI - 1 = [Cl^- - (Na^+ + K^+)]/Cl^- \quad (7)$$

$$CAI - 2 = [Cl^- - (Na^+ + K^+)]/(SO_4^{2-} + HCO_3^- + CO_3^{2-} + NO3_3^-) \quad (8)$$

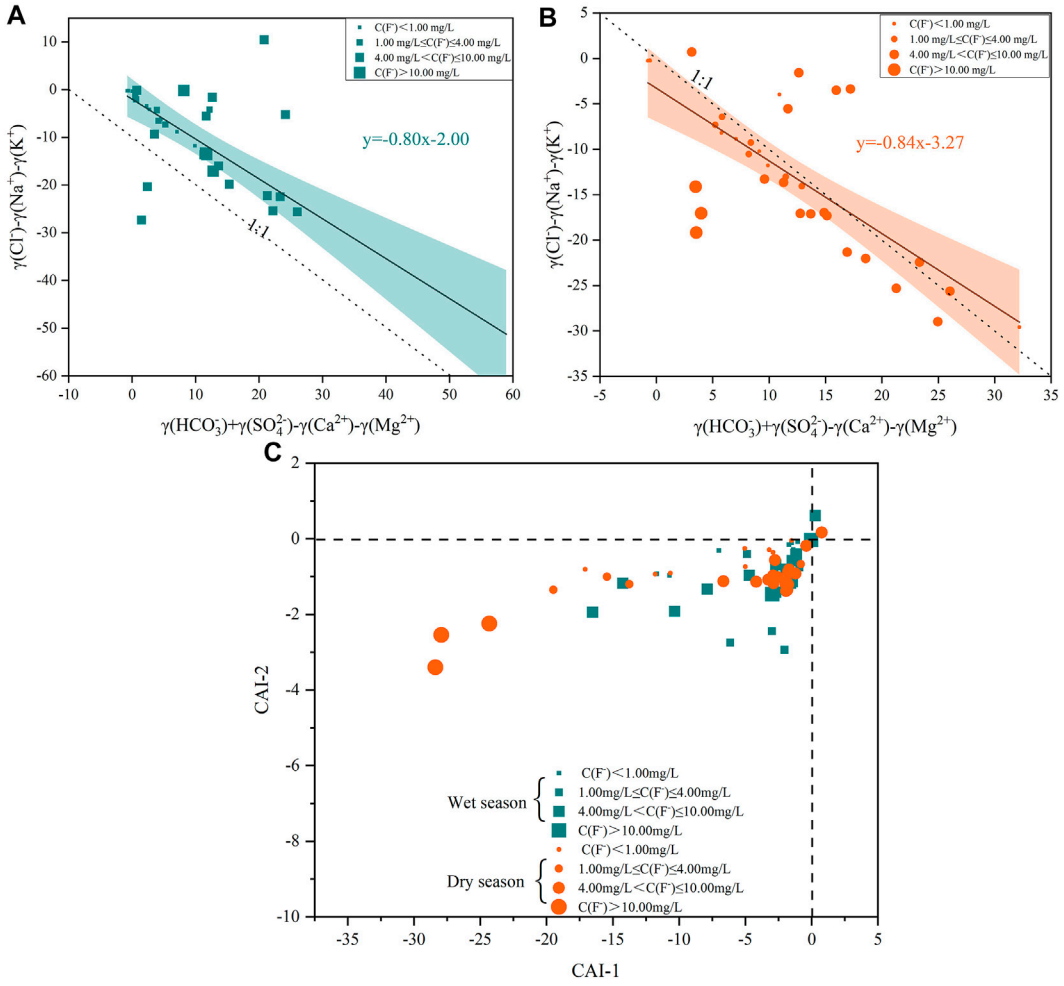

FIGURE 6
The plots of: **(A)** Cl^--Na^+-K^+ *versus* HCO_3^-+SO_4^{2-}-Ca^{2+}-Mg^{2+} during the wet season; **(B)** Cl^--Na^+-K^+ *versus* HCO_3^-+SO_4^{2-}-Ca^{2+}-Mg^{2+} during the dry season; **(C)** CAI-1 *versus* CAI-2 during the wet and dry season in deep groundwater.

As shown in Figure 6C, 94.28% and 97.14% of the deep groundwater samples show negative CAI 1 and CAI 2 values during the wet and dry season, respectively, indicating the Ca^{2+} and Mg^{2+} in the deep groundwater have been exchanged by K^+ and Na^+ in the stratum and explaining F^- enrichment in deep groundwater. In addition, the CAI 1 and CAI 2 absolute values of deep groundwater during the dry season was higher than that during the wet season, further implying that ion exchange interactions were more dominant. Thus, the cation exchange process primarily increases the F^- concentration in deep groundwater during the dry season (Li et al., 2015; Hao et al., 2022).

The TDS values exhibited a positive correlation with F^- in the study area during both dry and wet seasons (Figure 4D), indicating that an enhancement of ionic strength increased F^- concentrations in deep groundwater (Dehbandi et al., 2018; Wu et al., 2018; Laxmankumar et al., 2019). Atmospheric precipitation, evaporation, and rock weathering can reflect hydrogeochemical processes in Gibbs diagrams. All high-F^- deep groundwater samples from both the dry and wet seasons fell under rock weathering and evaporation dominance with medium to high TDS, high Na/(Na+Ca) and low Cl/(Cl+HCO_3) ratios (Supplementary Figure S2), indicating that the rock weathering and evaporation processes were dominant geochemical factors for increasing the F^- content in deep groundwater (Dehbandi et al., 2018; LaFayette et al., 2020; Hao et al., 2021d).

Irrigation water quality

The irrigation water quality was thoroughly assessed and the results are presented in Figure 7. The United States salinity hazard diagram (Figure 7A) illustrated that 25.71%, 14.29%,

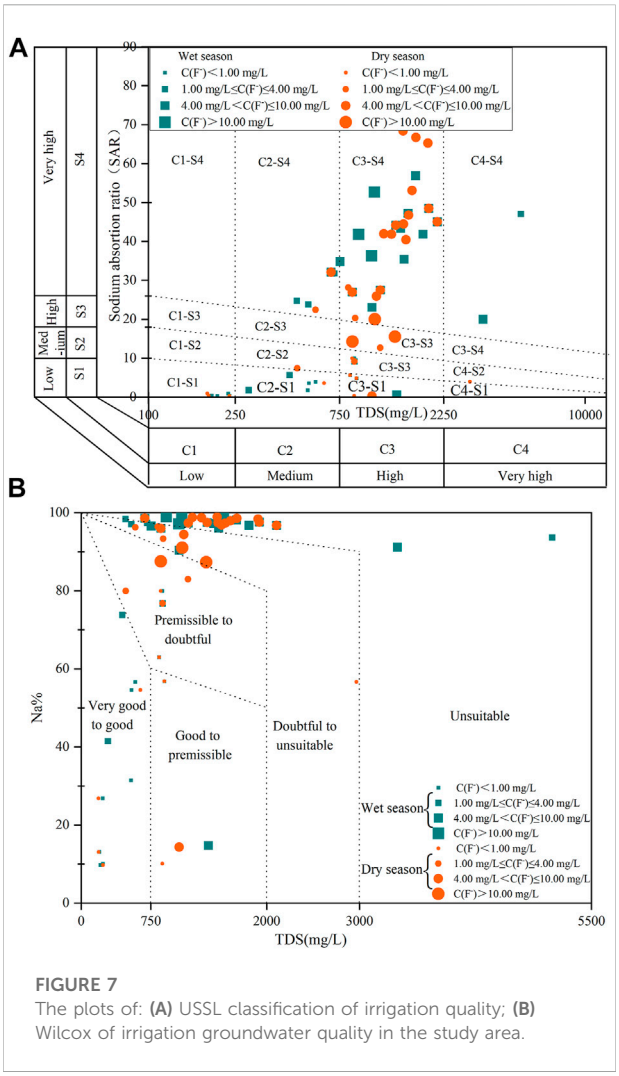

FIGURE 7
The plots of: **(A)** USSL classification of irrigation quality; **(B)** Wilcox of irrigation groundwater quality in the study area.

40.00%, and 5.71% of deep groundwater samples in the wet season fell in zones with low salinity and alkalinity, medium salinity and low and very high alkalinity, high salinity and very high alkalinity, and very high salinity and alkalinity, respectively. Similarly, 14.29%, 25.71%, 57.14%, and 2.86% of deep groundwater samples in the dry season were found in C1-S1, C2-S1-S2-S4, C3-S1-S2-S3-S4, and C4-S2 zones, indicating low salinity and alkalinity; medium salinity and low, medium, and very high alkalinity; high salinity and all alkalinity; and very high salinity and medium alkalinity, respectively.

Wilcox plots (Figure 7B) revealed that 100% and 88.89% of low-F^- deep groundwater samples fell in the very good to good field during the wet and dry seasons, respectively, indicating that most low-F^- deep groundwater samples had excellent irrigation water quality. However, 84.00% and 84.62% of high-F^- deep groundwater samples fell in the doubtful to unsuitable and unsuitable fields during the wet and dry seasons, respectively. With increasing F^- concentration, deep groundwater samples significantly diverged from suitable to unsuitable irrigation fields, indicating that F^- concentration in deep groundwater was a key variable in determining ecological risk in the study area.

Conclusion

In this study, we highlighted F^- contamination in deep groundwater in the vicinity of the Shendong mining area during the wet and dry seasons. A total of 65.71% (wet season) and 74.29% (dry season) of deep groundwater samples exhibited F^- concentrations exceeding the limit set by the drinking water guideline in China (1.00 mg/L). In addition, the mean F^- concentrations in deep groundwater were higher during the dry season than those during the wet season. The spatial distribution of F^- in deep groundwater was stable during both dry and wet seasons, with a noticeable increase from southeast to northwest.

Several geochemical processes, including the dissolution and precipitation of F^--bearing and calcium minerals, cation exchange, competitive adsorption, evaporation, and anthropogenic activities during both the wet and dry seasons, may have contributed to the F^- enrichment of deep groundwater. Importantly, the precipitation of dolomite, cation exchange, competitive adsorption, and mining activities may have been the primary causes of the seasonal differences in F^- content.

The risk of high-F^- deep groundwater to the ecological environment in the study area was assessed, and the results indicated that 100% and 88.89% of low-F^- deep groundwater samples had excellent irrigation water quality during the wet and dry seasons, respectively. However, at the same time, 84.00% and 84.62% of high-F^- deep groundwater samples were unsuitable for irrigation during the wet and dry seasons, respectively. The F^- concentration in deep groundwater was a key influential variable for ecological risk in the study area. Therefore, it is essential to devise effective pretreatment methods of minimizing the risk of the deep groundwater fluoride such as ion exchange, membrane separation, electrodialysis, precipitation, reverse osmosis, and adsorption before ecological irrigation.

Despite F^- enriched in deep groundwater during the wet and dry season, the influence of seasonal fluctuation of groundwater level on the formation of high fluoride water was not deeply discussed in the article. In addition, our findings are not assessed health risk for few rural residents and limited to promote the local govern management of deep groundwater resources within the study area. Hence, the studies will aid in the development of policies aimed at preventing high levels of F^- in deep groundwater in the study area, to protect the ecological environment and gain a better understanding of the seasonal distribution and

geochemical factors of F^- in deep groundwater in the vicinity of the Shendong mining area.

Data availability statement

The datasets presented in this study can be found in online repositories. The names of the repository/repositories and accession number(s) can be found in the article/ Supplementary Material.

Author contributions

Conceptualization, methodology, and writing- original draft preparation, CH; data curation, visualization, and investigation, YW; software and investigation, KH; supervision, writing-reviewing, and editing, HG. All authors contributed to manuscript revision, read, and approved the submitted version.

Funding

This work was supported by the Natural Science Foundation of Hebei Province (D2021508004), Open Fund of Key Laboratory of Mine Water Resource Utilization of Anhui Higher Education Institutes, Suzhou University (Grant No. KMWRU202101), and Open Fund of State Key Laboratory of Coal Resources and Safe Mining (Grant No. SKLCRSM22KFA03).

Acknowledgments

We would like to thank Editage (www.editage.cn) for English language editing.

Conflict of interest

The authors declare that the research was conducted in the absence of any commercial or financial relationships that could be construed as a potential conflict of interest.

Publisher's note

All claims expressed in this article are solely those of the authors and do not necessarily represent those of their affiliated organizations, or those of the publisher, the editors and the reviewers. Any product that may be evaluated in this article, or claim that may be made by its manufacturer, is not guaranteed or endorsed by the publisher.

Supplementary material

The Supplementary Material for this article can be found online at: https://www.frontiersin.org/articles/10.3389/fenvs.2022.1024797/full#supplementary-material

References

Adeyeye, O. A., Xiao, C., Zhang, Z., Yawe, A. S., and Liang, X. (2021). Groundwater fluoride chemistry and health risk assessment of multi-aquifers in Jilin Qianan, Northeastern China. *Ecotoxicol. Environ. Saf.* 211, 111926. doi:10.1016/j.ecoenv.2021.111926

Aghapour, S., Bina, B., Tarrahi, M. J., Amiri, F., and Ebrahimi, A. (2018). Distribution and health risk assessment of natural fluoride of drinking groundwater resources of Isfahan, Iran, using GIS. *Environ. Monit. Assess.* 190 (3), 137. doi:10.1007/s10661-018-6467-z

Ali, S., Shekhar, S., Bhattacharya, P., Verma, G., Chandrasekhar, T., and Chandrashekhar, A. K. (2018). Elevated fluoride in groundwater of Siwani Block, Western Haryana, India, A potential concern for sustainable water supplies for drinking and irrigation. *Groundw. Sustain. Dev.* 7, 410–420. doi:10.1016/j.gsd.2018.05.008

Ali, W., Aslam, M. W., Junaid, M., Ali, K., Guo, Y., Rasool, A., et al. (2019). Elucidating various geochemical mechanisms drive fluoride contamination in unconfined aquifers along the major rivers in Sindh and Punjab, Pakistan. *Environ. Pollut.* 249, 535–549. doi:10.1016/j.envpol.2019.03.043

Araya, D., Podgorski, J., Kumi, M., Mainoo, P. A., and Berg, M. (2022). Fluoride contamination of groundwater resources in Ghana, Country-wide hazard modeling and estimated population at risk. *Water Res.* 212, 118083. doi:10.1016/j.watres.2022.118083

Blasco, M., Auqué, L. F., and Gimeno, M. J. (2019). Geochemical evolution of thermal waters in carbonate – evaporitic systems, the triggering effect of halite dissolution in the dedolomitisation and albitisation processes. *J. Hydrol. X.* 570, 623–636. doi:10.1016/j.jhydrol.2019.01.013

Borzi, G. E., Garcia, L., and Carol, E. S. (2015). Geochemical processes regulating F^-, as and NO_3^- content in the groundwater of a sector of the Pampean Region. *Argent. Sci. Total Environ.* 530-531, 154–162. doi:10.1016/j.scitotenv.2015.05.072

Chen, J., Gao, Y., Qian, H., Ren, W., and Qu, W. (2021). Hydrogeochemical evidence for fluoride behavior in groundwater and the associated risk to human health for a large irrigation plain in the Yellow River Basin. *Sci. Total Environ.* 800, 149428. doi:10.1016/j.scitotenv.2021.149428

Chicas, S. D., Omine, K., Prabhakaran, M., Sunitha, T. G., and Sivasankar, V. (2022). High fluoride in groundwater and associated non-carcinogenic risks at Tiruvannamalai region in Tamil Nadu, India. *Ecotoxicol. Environ. Saf.* 233, 113335. doi:10.1016/j.ecoenv.2022.113335

Currell, M., Cartwright, I., Raveggi, M., and Han, D. (2011). Controls on elevated fluoride and arsenic concentrations in groundwater from the Yuncheng Basin, China. *Appl. Geochem.* 26 (4), 540–552. doi:10.1016/j.apgeochem.2011.01.012

Dehbandi, R., Moore, F., and Keshavarzi, B. (2018). Geochemical sources, hydrogeochemical behavior, and health risk assessment of fluoride in an endemic fluorosis area, central Iran. *Chemosphere* 193, 763–776. doi:10.1016/j.chemosphere.2017.11.021

Duan, L., Wang, X., and Sun, Y. (2021). Occurrence characteristics and ecological risk assessment of fluorine in coal gangue. *Coal Convers.* 44 (2), 1–10. doi:10.19726/j.cnki.ebcc.202102011

Duggal, V., and Sharma, S. (2022). Fluoride contamination in drinking water and associated health risk assessment in the Malwa Belt of Punjab, India. *Environ. Adv.* 8, 100242. doi:10.1016/j.envadv.2022.100242

Eang, K. E., Igarashi, T., Kondo, M., Nakatani, T., Tabelin, C. B., and Fujinaga, R. (2018). Groundwater monitoring of an open-pit limestone quarry, Water-rock interaction and mixing estimation within the rock layers by geochemical and statistical analyses. *Int. J. Min. Sci. Technol.* 28 (6), 849–857. doi:10.1016/j.ijmst.2018.04.002

Emenike, C. P., Tenebe, I. T., and Jarvis, P. (2018). Fluoride contamination in groundwater sources in Southwestern Nigeria, Assessment using multivariate statistical approach and human health risk. *Ecotoxicol. Environ. Saf.* 156, 391–402. doi:10.1016/j.ecoenv.2018.03.022

Gu, D., Li, J., and Cao, Z. (2021). Technology and engineering development strategy of water protection and utilization of coal mine in China. *J. China Coal Soc.* doi:10.13225/j.cnki.jccs.2021.0917

Gu, D. Z. (2014). Water resource protection and utilization engineering technology of coal mining in "energy golden triangle" region. *Coal Eng.* 46 (10), 33–37. doi:10.11799/ce201410008

Guo, H., and Wang, Y. (2005). Geochemical characteristics of shallow groundwater in Datong basin, northwestern China. *J. Geochem. Explor.* 87 (3), 109–120. doi:10.1016/j.gexplo.2005.08.002

Guo, H., Zhang, Y., Xing, L., and Jia, Y. (2012). Spatial variation in arsenic and fluoride concentrations of shallow groundwater from the town of Shahai in the Hetao basin, Inner Mongolia. *Appl. Geochem.* 27 (11), 2187–2196. doi:10.1016/j.apgeochem.2012.01.016

Guo, Y., Yang, J., Zhang, Z., Li, G., Ting, L., and Wang, L. (2021). Hydrogen and oxygen isotope characteristics of mine water in the Shendong mine area and water-rock reactions mechanism of the formation of high-fluoride mine water. *J. China Coal Soc.* 46 (S2), 948–959. doi:10.13225/j.cnki.jccs.2021.0388

Hao, C., Liu, M., Peng, Y., and Wei, Z. (2021d). Comparison of antimony sources and hydrogeochemical processes in shallow and deep groundwater near the xikuangshan mine, hunan province, China. *Mine Water Environ.* 41 (1), 194–209. doi:10.1007/s10230-021-00833-8

Hao, C., Liu, M., Zhang, W., He, P., Lin, D., and Gui, H. (2021a). Spatial distribution, source identification, and health risk assessment of fluoride in the drinking groundwater in the Sulin coal district, northern Anhui Province, China. *Water Supply* 21 (5), 2444–2462. doi:10.2166/ws.2021.048

Hao, C., Sun, X., Xie, B., and Hou, S. (2022). Increase in fluoride concentration in mine water in Shendong mining area, Northwest China, Insights from isotopic and geochemical signatures. *Ecotoxicol. Environ. Saf.* 236, 113496. doi:10.1016/j.ecoenv.2022.113496

Hao, C., Zhang, W., and Gui, H. (2021b). Geochemical behaviours and formation mechanisms for elevated fluoride in the drinking groundwater in sulin coal-mining district, northern Anhui province, China. *Pol. J. Environ. Stud.* 30 (4), 3565–3578. doi:10.15244/pjoes/131193

Hao, C., Zhang, W., and He, R. (2021c). Formation mechanisms for elevated fluoride in the mine water in Shendong coal-mining district. *J. China Coal Soc.* 46 (6), 1966–1977. doi:10.13225/j.cnki.jccs.ST21.0160

He, J., An, Y., and Zhang, F. (2013). Geochemical characteristics and fluoride distribution in the groundwater of the Zhangye Basin in Northwestern China. *J. Geochem. Explor.* 135, 22–30. doi:10.1016/j.gexplo.2012.12.012

He, X., Ma, T., Wang, Y., Shan, H., and Deng, Y. (2013). Hydrogeochemistry of high fluoride groundwater in shallow aquifers, Hangjinhouqi, Hetao Plain. *J. Geochem. Explor.* 135, 63–70. doi:10.1016/j.gexplo.2012.11.010

Huang, L., Sun, Z., Zhou, A., Bi, J., and Liu, Y. (2022). Source and enrichment mechanism of fluoride in groundwater of the hotan oasis within the tarim basin, northwestern China. *Environ. Pollut.* 300, 118962. doi:10.1016/j.envpol.2022.118962

Jakóbczyk-Karpierz, S., Sitek, S., Jakobsen, R., and Kowalczyk, A. (2017). Geochemical and isotopic study to determine sources and processes affecting nitrate and sulphate in groundwater influenced by intensive human activity - carbonate aquifer Gliwice (southern Poland). *Appl. Geochem.* 76, 168–181. doi:10.1016/j.apgeochem.2016.12.005

Jeong, S. W., Wu, Y. H., Cho, Y. C., and Ji, S. W. (2018). Flow behavior and mobility of contaminated waste rock materials in the abandoned Imgi mine in Korea. *Geomorphology* 301, 79–91. doi:10.1016/j.geomorph.2017.10.021

Kumar, P., Singh, C. K., Saraswat, C., Mishra, B., and Sharma, T. (2019). Evaluation of aqueous geochemistry of fluoride enriched groundwater, A case study of the Patan district, Gujarat, Western India. *Water Sci.* 31 (2), 215–229. doi:10.1016/j.wsj.2017.05.002

Kumar, S., Venkatesh, A. S., Singh, R., Udayabhanu, G., and Saha, D. (2018). Geochemical signatures and isotopic systematics constraining dynamics of fluoride contamination in groundwater across Jamui district, Indo-Gangetic alluvial plains, India. *Chemosphere* 205, 493–505. doi:10.1016/j.chemosphere.2018.04.116

LaFayette, G. N., Knappett, P. S. K., Li, Y., Loza-Aguirre, I., and Polizzotto, M. L. (2020). Geogenic sources and chemical controls on fluoride release to groundwater in the Independence Basin, Mexico. *Appl. Geochem.* 123, 104787. doi:10.1016/j.apgeochem.2020.104787

Laxmankumar, D., Satyanarayana, E., and Dhakate, R. (2019). Hydrogeochemical characteristics with respect to fluoride contamination in groundwater of Maheshwarm mandal, RR district, Telangana state, India. *Groundw. Sustain. Dev.* 8, 474–483. doi:10.1016/j.gsd.2019.01.008

Li, C., Gao, X., and Wang, Y. (2015). Hydrogeochemistry of high-fluoride groundwater at Yuncheng Basin, northern China. *Sci. Total Environ.* 508, 155–165. doi:10.1016/j.scitotenv.2014.11.045

Li, D., Gao, X., Wang, Y., and Luo, W. (2018). Diverse mechanisms drive fluoride enrichment in groundwater in two neighboring sites in northern China. *Environ. Pollut.* 237, 430–441. doi:10.1016/j.envpol.2018.02.072

Li, Y., Bi, Y., Mi, W., Xie, S., and Ji, L. (2021). Land-use change caused by anthropogenic activities increase fluoride and arsenic pollution in groundwater and human health risk. *J. Hazard. Mat.* 406, 124337. doi:10.1016/j.jhazmat.2020.124337

Liu, J., Peng, Y., Li, C., Gao, Z., and Chen, S. (2021). A characterization of groundwater fluoride, influencing factors and risk to human health in the southwest plain of Shandong Province, North China. *Ecotoxicol. Environ. Saf.* 207, 111512. doi:10.1016/j.ecoenv.2020.111512

Mamatchi, M., Rajendran, R., Lumo, A. K., Arumugam, G., Kpemissi, M., Sadikou, A., et al. (2019). Cardiovascular dysfunction and oxidative stress following human contamination by fluoride along with environmental xenobiotics (Cd & Pb) in the phosphate treatment area of Togo, West Africa. *J. Trace Elem. Med. Biol.* 56, 13–20. doi:10.1016/j.jtemb.2019.07.002

Mondal, D., Gupta, S., Reddy, D. V., and Nagabhushanam, P. (2014). Geochemical controls on fluoride concentrations in groundwater from alluvial aquifers of the Birbhum district, West Bengal, India. *J. Geochem. Explor.* 145, 190–206. doi:10.1016/j.gexplo.2014.06.005

Mwiathi, N. F., Gao, X., Li, C., and Rashid, A. (2022). The occurrence of geogenic fluoride in shallow aquifers of Kenya Rift Valley and its implications in groundwater management. *Ecotoxicol. Environ. Saf.* 229, 113046. doi:10.1016/j.ecoenv.2021.113046

Najamuddin, T. P., Sanusi, H. S., and Nurjaya, I. W. (2016). Seasonal distribution and geochemical fractionation of heavy metals from surface sediment in a tropical estuary of Jeneberang River, Indonesia. *Mar. Pollut. Bull.* 111 (1-2), 456–462. doi:10.1016/j.marpolbul.2016.06.106

Nizam, S., Virk, H. S., and Sen, I. S. (2022). High levels of fluoride in groundwater from Northern parts of Indo-Gangetic plains reveals detrimental fluorosis health risks. *Environ. Adv.* 8, 100200. doi:10.1016/j.envadv.2022.100200

Noor, S., Rashid, A., Javed, A., Khattak, J. A., and Farooqi, A. (2022). Hydrogeological properties, sources provenance, and health risk exposure of fluoride in the groundwater of Batkhela, Pakistan. *Environ. Technol. Innov.* 25, 102239. doi:10.1016/j.eti.2021.102239

Olaka, L. A., Wilke, F. D., Olago, D. O., Odada, E. O., Mulch, A., and Musolff, A. (2016). Groundwater fluoride enrichment in an active rift setting, Central Kenya Rift case study. *Sci. Total Environ.* 545-546, 641–653. doi:10.1016/j.scitotenv.2015.11.161

Orland, I. J., Burstyn, Y., Bar-Matthews, M., Kozdon, R., Ayalon, A., Matthews, A., et al. (2014). Seasonal climate signals (1990–2008) in a modern Soreq Cave stalagmite as revealed by high-resolution geochemical analysis. *Chem. Geol.* 363, 322–333. doi:10.1016/j.chemgeo.2013.11.011

Rafique, T., Naseem, S., Ozsvath, D., Hussain, R., Bhanger, M. I., and Usmani, T. H. (2015). Geochemical controls of high fluoride groundwater in umarkot sub-district, thar desert, Pakistan. *Sci. Total Environ.* 530-531, 271–278. doi:10.1016/j.scitotenv.2015.05.038

Rashid, A., Guan, D. X., Farooqi, A., Khan, S., Zahir, S., Jehan, S., et al. (2018). Fluoride prevalence in groundwater around a fluorite mining area in the flood plain of the River Swat, Pakistan. *Sci. Total Environ.* 635, 203–215. doi:10.1016/j.scitotenv.2018.04.064

Rehman, F., Siddique, J., Shahab, A., Azeem, T., Bangash, A. A., Naseem, A. A., et al. (2022). Hydrochemical appraisal of fluoride contamination in groundwater and human health risk assessment at Isa Khel, Punjab, Pakistan. *Environ. Technol. Innov.* 27, 102445. doi:10.1016/j.eti.2022.102445

Sahu, M., Sar, S. K., Baghel, T., and Dewangan, R. (2020). Seasonal and geochemical variation of uranium and major ions in groundwater at Kanker district of Chhattisgarh, central India. *Groundw. Sustain. Dev.* 10, 100330. doi:10.1016/j.gsd.2020.100330

Singh, A. K., Mahato, M. K., Neogi, B., Mondal, G. C., and Singh, T. B. (2011). Hydrogeochemistry, elemental flux, and quality assessment of mine water in the pootkee-balihari mining area, jharia coalfield, India. *Mine Water Environ.* 30 (3), 197. doi:10.1007/s10230-011-0143-7

Song, H., Xu, J., Fang, J., Cao, Z., Yang, L., and Li, T. (2020). Potential for mine water disposal in coal seam goaf, Investigation of storage coefficients in the Shendong mining area. *J. Clean. Prod.* 244, 118646. doi:10.1016/j.jclepro.2019.118646

Su, H., Kang, W., Li, Y., and Li, Z. (2021). Fluoride and nitrate contamination of groundwater in the Loess Plateau, China, Sources and related human health risks. *Environ. Pollut.* 286, 117287. doi:10.1016/j.envpol.2021.117287

Thapa, R., Gupta, S., Gupta, A., Reddy, D. V., and Kaur, H. (2018). Geochemical and geostatistical appraisal of fluoride contamination, an insight into the Quaternary aquifer. *Sci. Total Environ.* 640-641, 406–418. doi:10.1016/j.scitotenv.2018.05.360

Toolabi, A., Bonyadi, Z., Paydar, M., Najafpoor, A. A., and Ramavandi, B. (2021). Spatial distribution, occurrence, and health risk assessment of nitrate, fluoride, and arsenic in Bam groundwater resource, Iran. *Groundw. Sustain. Dev.* 12, 100543. doi:10.1016/j.gsd.2020.100543

Wang, B., Xu, H., Wang, D., and He, S. (2021). The influence mechanism of HCO_3^- on fluoride removal by different types of aluminum salts. *Colloids Surfaces A Physicochem. Eng. Aspects* 126124. doi:10.1016/j.colsurfa.2020.126124

Wu, C., Wu, X., Qian, C., and Zhu, G. (2018). Hydrogeochemistry and groundwater quality assessment of high fluoride levels in the Yanchi endorheic region, northwest China. *Appl. Geochem.* 98, 404–417. doi:10.1016/j.apgeochem.2018.10.016

Xiao, J., Jin, Z., and Zhang, F. (2015). Geochemical controls on fluoride concentrations in natural waters from the middle Loess Plateau, China. *J. Geochem. Explor.* 159, 252–261. doi:10.1016/j.gexplo.2015.09.018

Xiao, W., Lv, X., Zhao, Y., Sun, H., and Li, J. (2020). Ecological resilience assessment of an arid coal mining area using index of entropy and linear weighted analysis, A case study of Shendong Coalfield, China. *Ecol. Indic.* 109, 105843. doi:10.1016/j.ecolind.2019.105843

Xu, J., Zhu, W., Xu, J., Wu, J., and Li, Y. (2021). High-intensity longwall mining-induced ground subsidence in Shendong coalfield, China. *Int. J. Rock Mech. Min. Sci.* 141, 104730. doi:10.1016/j.ijrmms.2021.104730

Yadav, K., Raphi, M., and Jagadevan, S. (2021). Geochemical appraisal of fluoride contaminated groundwater in the vicinity of a coal mining region, Spatial variability and health risk assessment. *Geochemistry* 81 (1), 125684. doi:10.1016/j.chemer.2020.125684

Yang, Z., Li, W., Li, X., Wang, Q., and He, J. (2019). Assessment of eco-geo-environment quality using multivariate data, A case study in a coal mining area of Western China. *Ecol. Indic.* 107, 105651. doi:10.1016/j.ecolind.2019.105651

Yuan, S., Sui, W., Han, G., and Duan, W. (2022). *An optimized combination of mine water control, treatment, utilization, and reinjection for environmentally sustainable mining, A case study. Mine Water Environ.* 41 (3) 828–839. doi:10.1007/s10230-022-00886-3

Zango, M. S., Pelig-Ba, K. B., Anim-Gyampo, M., Gibrilla, A., and Sunkari, E. D. (2021). Hydrogeochemical and isotopic controls on the source of fluoride in groundwater within the Vea catchment, northeastern Ghana. *Groundw. Sustain. Dev.* 12, 100526. doi:10.1016/j.gsd.2020.100526

Zhang, J., Chen, L., Hou, X., Ren, X., Li, J., and Chen, Y. (2022). Hydrogeochemical processes of carboniferous limestone groundwater in the yangzhuang coal mine, huaibei coalfield, China. *Mine Water Environ.* 41 (2), 504–517. doi:10.1007/S10230-022-00861-Y

Zhang, Z., Li, G., Su, X., Zhuang, X., Wang, L., Fu, H., et al. (2021). Geochemical controls on the enrichment of fluoride in the mine water of the Shendong mining area, China. *Chemosphere* 284, 131388. doi:10.1016/j.chemosphere.2021.131388

Zhao, B., and Wei, N. (2020). Study on content distribution and occurrenceform of fluorine in Shaanxi coal. *Coal Qual. Technol.* 35 (6), 34–39.